Advances in Nano Research, *Vol. 13, No. 2 (2022) 113-120*
https://doi.org/10.12989/anr.2022.13.2.113

Assessment of nonlinear stability of geometrically imperfect nanoparticle-reinforced beam based on numerical method

Yuxin Zheng, Hongwei Jin* and Congying Jiang

School of Civil Engineering and Architecture, Zhejiang Guangsha Vocational and Technical University of Construction, Dongyang 322100, Zhejiang, China

(*Received July 1, 2021, Revised August 11, 2021, Accepted November 17, 2021*)

Abstract. In this paper, a finite element (FE) simulation has been developed in order to examine the nonlinear stability of reinforced sandwich beams with graphene oxide powders (GOPs). In this regard, the nonlinear stability curves have been obtained asuming that the beam is under compressive loads leading to its buckling. The beam is considered to be a three-layered sandwich beam with metal core and GOP reinforced face sheets and it is rested on elastic substrate. Moreover, a higher-order refined beam theory has been considered to formulate the sandwich beam by employing the geometrically perfect and imperfect beam configurations. In the solving procedure, the utalized finite element simulation contains a novel beam element in which shear deformation has been included. The calculated stability curves of GOP-reinforced sandwich beams are shown to be dependent on different parameters such as GOP amount, face sheet thickness, geometrical imperfection and also center deflection.

Keywords: finite element method; nonlinear stability; numerical simulation; sandwich beam

1. Introduction

In recent decades, several carbon based structures containing carbon nanotube or carbon fiber have been widely utilized in composites for enhancing their mechanics and thermal specifications (Keleshtreri *et al*. 2016). A 273% enhancement of elastic modulus is obtained by Ahankari *et al*. (2010) for carbon reinforced composites in comparison to conventional composites. Likewise, Gojny *et al*. (2004) mentioned that structural stiffness of carbon based composites may be enhanced with incorporation of carbon nanotube within material. Impacts of configuration and scale of carbon nanotubes on rigidity growth of material composites having metallic matrices are studied by Esawi *et al*. (2011). Regarding to the offering above explained properties, beams and plates having carbon-based nanofiller are inquired to determine their static or dynamical behaviors (Yang *et al*. 2017). There are also other studies on composite or functionally graded materials and concerned readers are refaced to those published papers on material science (Ebrahimi and Barati 2018a, b, c, d, e, f, g, h, Barati and Shahverdi 2017, Barati and Shahverdi 2018a, b, Shariati *et al*. 2020a, b, Abdulrazzaq *et al*. 2020, Mirjavadi *et al*. 2020a, b, c, d, e, f, g, h, i, j, k, l, Forsat *et al*. 2020). Likewise, the graphene based composite material has been recently gained enormous attentions because of having easy producing procedure and high rigidity growth. Nieto *et al*. (2017) presented a review paper based on several graphene based composite material possessing ceramic or metallic matrices. The multi-scale study of mechanical attributes for graphene based composite material has been provided by Lin *et al*. (2018) utilizing finite elements approach.

Until now, many researches are devoted to material characterization and mechanical properties estimation (Mou and Bai 2018, Yan *et al*. 2020, Ji *et al*. 2022, Ma *et al*. 2022, Xiong *et al*. 2020, Xiao *et al*. 2022). Many of researches in the fields of nano-composites have been interested in production and materials characteristics recognition of graphene based composites and structural components containing slight percentages of graphene fillers. For instance, it is mentioned by Rafiee *et al*. (2009) that some material characteristics of graphene based composites may be enhanced via placing 0.1% volume of graphene filler. However, achieving to this level of reinforcement employing nanotubes required 1% of their volume. Graphene based composites containing epoxy matrix were created by King *et al*. (2013) by placing 6% weight fraction of graphene fillers to polymeric phases. It was stated that Young modulus of the composite has been increased from 2.72 GPa to 3.36 GPa. Next, 57% increment for Young modulus has been achieved by Fang *et al*. (2009) based on a sample of graphene based composite.

Moreover, many studies in the fields of nano-mechanic are associated with vibrational and stability investigation of various structural elements containing beam or plate reinforced via diverse carbon-based dispersions. Vibrational properties of a laminated graphene based plate have been explored by Song *et al*. (2017) assuming simply support edge condition. They assumed that the plate is constructed from particular numbers of layers each containing a sensible content of graphene. Selecting a perturbation approach, static deflections and bucking loads of graphene based plates have been derived by Shen *et al*. (2017). In above papers, each material property has discontinuous variation across the thickness of beam or plate. Also, geometrically

*Corresponding author, Ph.D.,
E-mail: bcw2013@126.com

Copyright © 2022 Techno-Press, Ltd.

ISSN: 2287-237X (Print), 2287-2388 (Online)

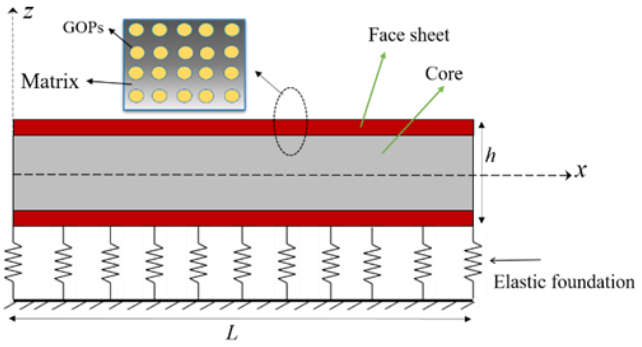

Fig. 1 A sandwich beam with GOP-reinforced face sheets resting on elastic foundation

nonlinear vibration frequencies of graphene based beams having embedded graphene have been explored by Feng *et al*. (2017) selecting first-order beam theory. Moreover, vibration frequencies of graphene based beams having porosities have been explored by Kitipornchai *et al*. (2017).

Recently, reinforcement of materials with nano-size inclusions is a novel case study. Many researches show that mechanical properties of materials can be enhanced by adding graphene platelets (GPLs), graphene oxide powders (GOPs) and ever carbon nanotubes (Du *et al*. 2016). Graphene oxide, formed from graphene, is extensively and economically accessible from graphite mass oxidation. It is compatible with many matrix materials including polymeric materials and even concrete (Mohammed *et al*. 2017). A graphene oxide composite illustrates large elastic modulus and tensile strength because it is a carbon-filled material having promising performances with low costs (Zhang *et al*. 2020). To the best of author's knowledge, post-buckling study of geometrically imperfect sandwich beams reinforced by GOPs is not performed yet.

The present research is devoted to develop a finite element (FE) simulation in order to examine the nonlinear stability of reinforced sandwich beams with graphene oxide powders (GOPs). In this regard, the nonlinear stability curves have been obtained asuming that the beam is under in-plane mechanical load leading to its buckling. The beam is considered to be a three-layered sandwich beam with metal core and GOP reinforced face sheets. Moreover, a higher-order refined beam theory has been considered to formulate the sandwich beam by employing the geometrically perfect and imperfect beam configurations. In the solving procedure, the utalized finite element simulation contains a novel beam element in which shear deformation has been included. The calculated stability curves of GOP-reinforced sandwich beams are shown to be dependent on different parameters such as GOP amount, face sheet thickness, geometrical imperfection and also center deflection.

2. GOP-based composites

According to Fig. 1, it is assumed that GOPs have uniform dispersion within the structure. In this figure, a GOP reinforced sandwich beam is illustrated. The total thickess is $h=h_c+2h_f$ where h_c and h_f are core thickness and face sheet thickness, respectively. Micro-mechanic theory of such composite materials introduces the below relationship between GOPs weight fraction (F_{GOP}) and their volume fraction (V_{GOP}) by:

$$\boldsymbol{V^{*}_{GOP}=\frac{F_{GOP}}{F_{GOP}+\frac{\rho_{GOP}}{\rho_M}-\frac{\rho_{GOP}}{\rho_M}F_{GOP}}} \tag{1}$$

where ρ_{GOP} and ρ_M define the mass densities of GOP and matrices, respectively. Next, the elastic modulus of a GOP based composite might be represented based upon matrix elastic modulus (E_M) by:

$$\begin{aligned}\boldsymbol{E_1=0.49\left(\frac{1+\xi_L^{GOP}\eta_L^{GOP}V_{GOP}}{1-\eta_L^{GOP}V_{GOP}}\right)E_M}\\ \boldsymbol{+0.51\left(\frac{1+\xi_W^{GOP}\eta_W^{GOP}V_{GOP}}{1-\eta_W^{GOP}V_{GOP}}\right)E_M}\end{aligned} \tag{2}$$

so that ξ_L^{GOP} and ξ_W^{GOP} define two geometrical factors indicating the impacts of graphene configuration and scales as:

$$\xi_L^{GOP}=\frac{2d_{GOP}}{t_{GOP}} \tag{3a}$$

$$\eta_L^{GOP}=\frac{(E_{GOP}/E_M)-1}{(E_{GOP}/E_M)+\xi_L^{GOP}} \tag{3b}$$

$$\xi_W^{GOP}=\frac{2d_{GOP}}{t_{GOP}} \tag{3c}$$

$$\eta_W^{GOP}=\frac{(E_{GOP}/E_M)-1}{(E_{GOP}/E_M)+\xi_W^{GOP}} \tag{3d}$$

so that d_{GPL} and t_{GPL} define GOP average diameter and thickness, respectively. Furthermore, Poisson's ratio for GOP based composite might be defined based upon Poisson's ratio of the two constituents and thermal expansion coefficient (α_1) in the form:

$$v_1=v_{GOP}V_{GOP}+v_MV_M \tag{4}$$

in which $V_M=1-V_{GOP}$expresses the volume fractions of matrix component. In this research, the core layer of the beam is considered to be made of Aluminum and the face sheets are made of GOP-reinforced composites with epoxy matrix. The Young's modulus and Poisson's ration of the core have been denoted by E_c=70 GPa and v_c=0.34, respectively.

3. Beam modeling via refined theory

So far, a variety of beam theories are introduced for description and analyzes of beam structures (Ebrahimi and Barati 2017a, b, c, d, e, Fenjan *et al*. 2020a, b, Kunbar *et al*. 2020, Muhammad *et al*. 2019, Ahmed *et al*. 2020a, b). The displacement field containing axial displacement (u_1) and transverse displacement (u_3) with respect to the refined beam assumption calculating the precise location of the neutral axis might be defined as:

$$\boldsymbol{u_1(x,z)=u(x)-z\frac{\partial w_b}{\partial x}-f(z)\frac{\partial w_s}{\partial x}} \tag{7}$$

$$\boldsymbol{u_3(x,z) = w(x) = w_b(x) + w_s(x)} \tag{8}$$

where the present theory has a third-order function in the form:

$$f(z) = -\frac{z}{4} + \frac{5z^3}{3h^2} \tag{9}$$

and

$$g(z) = 1 - df/dz \tag{10}$$

Above displacement field is calculated form the axial displacement (u), together with $w_b$and $w_s$as bending and shear displacements. Accordingly, one may calculate the strains of as:

$$\begin{aligned} \varepsilon_x &= \frac{\partial u}{\partial x} + \frac{1}{2}(\frac{\partial w}{\partial x})^2 - z\frac{\partial^2 w_b}{\partial x^2} - f(z)\frac{\partial^2 w_s}{\partial x^2} \\ \gamma_{xz} &= g(z)\frac{\partial w_s}{\partial x} \end{aligned} \tag{11}$$

Also, the function of 'M' is also characterized as follows.

$$\widetilde{M}(x_i) = \prod_{j=1, j\neq i}^{n} (x_i - x_j) \tag{11}$$

Based on proposed beam model and using Hamilton's rule, one can express the governing equations of the GOP reinforced beam as follows:

$$\frac{\partial N_x}{\partial x} = 0 \tag{12}$$

$$\begin{aligned} &\frac{\partial^2 M_x^b}{\partial x^2} + \frac{\partial}{\partial x}(N_x\frac{\partial(w_b + w_s)}{\partial x}) \\ &= +k_L(w_b + w_s) - (k_P)\nabla^2(w_b + w_s) \\ &+k_{NL}(w_b + w_s)^3 = 0 \end{aligned} \tag{13}$$

$$\begin{aligned} &\frac{\partial^2 M_x^s}{\partial x^2} + \frac{\partial Q_{xz}}{\partial x} + \frac{\partial}{\partial x}(N_x\frac{\partial(w_b + w_s)}{\partial x}) \\ &-k_L(w_b + w_s) + (k_P)\nabla^2(w_b + w_s) \\ &-k_{NL}(w_b + w_s)^3 = 0 \end{aligned} \tag{14}$$

So that forces and moments might be calculated as:

$$\begin{aligned} &(N_x, M_x^b, M_x^s) \\ &= \int_{-h/2}^{h/2} (1, z - z^*, f - z^{**})\sigma_x\, dz, \\ &Q_{xz} = \int_{-h/2}^{h/2} g(z)\sigma_{xz}\, dz \end{aligned} \tag{15}$$

Also, k_L, k_p, and k_{NL} defines linear, shear and non-linear types of foundation; P is called applied load.

Taking into account geometric imperfection effect and with aid of Eq. (15), the relations for force-strain and the moment-strain might be derived:

$$N_x = A[\frac{\partial u}{\partial x} + \frac{1}{2}(\frac{\partial(w_b + w_s)}{\partial x})^2 - \frac{1}{2}(\frac{\partial(w_b^* + w_s^*)}{\partial x})^2] \tag{16}$$

$$M_x^b = -D(\frac{\partial^2 w_b}{\partial x^2} - \frac{\partial^2 w_b^*}{\partial x^2}) - E(\frac{\partial^2 w_s}{\partial x^2} - \frac{\partial^2 w_s^*}{\partial x^2}) \tag{17}$$

$$M_x^s = -E(\frac{\partial^2 w_b}{\partial x^2} - \frac{\partial^2 w_b^*}{\partial x^2}) - F(\frac{\partial^2 w_s}{\partial x^2} - \frac{\partial^2 w_s^*}{\partial x^2}) \tag{18}$$

$$Q_{xz} = A_s\frac{\partial w_s}{\partial x} \tag{19}$$

in which

$$\begin{aligned} A &= \int_{-h_c/2-h_f}^{-h_c/2} E_i\, dz + \int_{-h_c/2}^{h_c/2} E_c\, dz + \int_{h_c/2}^{h_c/2+h_f} E_i\, dz, \\ D &= \int_{-h_c/2-h_f}^{-h_c/2} E_i z\, dz + \int_{-h_c/2}^{h_c/2} E_c z\, dz + \int_{h_c/2}^{h_c/2+h_f} E_i z\, dz, \\ E &= \int_{-h_c/2-h_f}^{-h_c/2} E_i\, zf dz + \int_{-h_c/2}^{h_c/2} E_c\, zf dz + \int_{h_c/2}^{h_c/2+h_f} E_i\, zf dz, \\ F &= \int_{-h_c/2-h_f}^{-h_c/2} E_i f^2\, dz + \int_{-h_c/2}^{h_c/2} E_c\, f^2 dz + \int_{h_c/2}^{h_c/2+h_f} E_i\, f^2 dz, \\ A_s &= \int_{-h_c/2-h_f}^{-h_c/2} \frac{E_i}{2(1+v_i)} g^2\, dz + \int_{-h_c/2}^{h_c/2} \frac{E_c}{2(1+v_c)} g^2\, dz \\ &\quad + \int_{h_c/2}^{h_c/2+h_f} \frac{E_i}{2(1+v_i)} g^2\, dz, \end{aligned} \tag{20}$$

There are three nonlinear governing equations for proposed refined beam model which can be written with respect to displacements from inserting Eqs. (16)-(19), into Eqs. (12)-(14) as:

$$\begin{aligned} &A(\frac{\partial^2 u}{\partial x^2}) + A(\frac{\partial(w_b + w_s)}{\partial x}\frac{\partial^2(w_b + w_s)}{\partial x^2} \\ &+\frac{\partial(w_b^* + w_s^*)}{\partial x}\frac{\partial^2(w_b^* + w_s^*)}{\partial x^2}) = 0 \end{aligned} \tag{21}$$

$$\begin{aligned} &-D(\frac{\partial^4 w_b}{\partial x^4} - \frac{\partial^4 w_b^*}{\partial x^4}) - E(\frac{\partial^4 w_s}{\partial x^4} - \frac{\partial^4 w_s^*}{\partial x^4}) \\ &+\frac{\partial}{\partial x}(N_x\frac{\partial w}{\partial x}) - k_L(w_b + w_s - w_b^* - w_s^*) \\ &+k_P(\frac{\partial^2 w_b}{\partial x^2} - \frac{\partial^2 w_b^*}{\partial x^2} + \frac{\partial^2 w_s}{\partial x^2} - \frac{\partial^2 w_s^*}{\partial x^2}) \\ &-k_{NL}[(w_b + w_s)^3 - (w_b^* + w_s^*)^3] = 0 \end{aligned} \tag{22}$$

$$\begin{aligned} &-E(\frac{\partial^4 w_b}{\partial x^4} - \frac{\partial^4 w_b^*}{\partial x^4}) - F(\frac{\partial^4 w_s}{\partial x^4} - \frac{\partial^4 w_s^*}{\partial x^4}) \\ &+\frac{\partial}{\partial x}(N_x\frac{\partial w}{\partial x}) + A_{44}(\frac{\partial^2 w_s}{\partial x^2} - \frac{\partial^2 w_s^*}{\partial x^2}) \\ &-k_L(w_b + w_s - w_b^* - w_s^*) \\ &+k_P(\frac{\partial^2 w_b}{\partial x^2} - \frac{\partial^2 w_b^*}{\partial x^2} + \frac{\partial^2 w_s}{\partial x^2} - \frac{\partial^2 w_s^*}{\partial x^2}) \\ &-k_{NL}[(w_b + w_s)^3 - (w_b^* + w_s^*)^3] = 0 \end{aligned} \tag{23}$$

It is proved that the first derivative of axial displacement (u) based on $u(0)$=0, $u(L)$=-PL/A can be calculated as:

$$\begin{aligned} &\frac{\partial u}{\partial x} = -\frac{1}{2}(\frac{\partial(w_b + w_s)}{\partial x})^2 \\ &+\frac{1}{2}(\frac{\partial(w_b^* + w_s^*)}{\partial x})^2 + \frac{1}{2L}\int_0^L (\frac{\partial(w_b + w_s)}{\partial x})^2\, dx \\ &-\frac{1}{2L}\int_0^L (\frac{\partial(w_b^* + w_s^*)}{\partial x})^2\, dx - \frac{P}{A} \end{aligned} \tag{24}$$

The above expression can be place into the governing equations in order to eliminating axial displacement.

4. Solution by FEM

Through the present section, FEM has been selected for solving the buckling problem of a GOP based beam with geometric imperfection. For this goal, the refined beam element has been used with ten degrees of freedom. Herein, a shape function has been introduced for axial field component, and also Hermit shape function have been introduced for lateral field components which are:

$$u(x) = \sum_{i=1}^{2} U_i N_i(x) = N_1 U_1 + N_2 U_2 \tag{25}$$

$$w_b(x) = \sum_{i=1}^{4} a_i \widetilde{N}_i(x) = \widetilde{N}_1 W_{b1} + \widetilde{N}_2 W'_{b2} + \widetilde{N}_3 W_{b3} + \widetilde{N}_4 W'_{b4} \tag{26}$$

$$w_s(x) = \sum_{i=1}^{4} b_i \widetilde{N}_i(x) = \widetilde{N}_1 W_{s1} + \widetilde{N}_2 W'_{s2} + \widetilde{N}_3 W_{s3} + \widetilde{N}_4 W'_{s4} \tag{27}$$

So that U_i, a_i and b_i are field coefficients. Also, $a_i = \{W_{b1}, W'_{b2}, W_{b3}, W'_{b4}\}$ and $b_i = \{W_{s1}, W'_{s2}, W_{s3}, W'_{s4}\}$ and shape functions are:

$$N_1 = 1 - \frac{x}{L_e} \tag{28}$$

$$N_2 = \frac{x}{L_e} \tag{29}$$

$$\widetilde{N}_1 = \frac{1}{L_e^3}(2x^3 - 3x^2 L_e + L_e^3) \tag{30}$$

$$\widetilde{N}_2 = \frac{1}{L_e^3}(x^3 L_e - 2x^2 L_e^2 + x L_e^3) \tag{31}$$

$$\widetilde{N}_3 = \frac{1}{L_e^3}(-2x^3 + 3x^2 L_e) \tag{32}$$

$$\widetilde{N}_4 = \frac{1}{L_e^3}(x^3 L_e - x^2 L_e^2) \tag{33}$$

so that L_e defines the length for master element.

Placing Eqs. (25)-(27) in the weak form of the governing equations (H) and minimizing it to field coefficients U_i, W_{bi}, and W_{si} (Rezaiee-Pajand *et al*. 2018, Al-Maliki *et al*. 2019) results in below relation containing simultaneous algebraic equations:

$$\frac{\partial H}{\partial U_i} = \frac{\partial H}{\partial W_{bi}} = \frac{\partial H}{\partial W_{si}} = 0 \tag{34}$$

Then, by considering Eq. (34) two coupled nonlinear governing equation will be derived:

$$k_{1,1} W_b + k_{1,2} W_s + G^* \widetilde{W}^3 + \Psi_{1,1} W_b^* + \Psi_{1,2} W_s^* = 0 \tag{35}$$

$$k_{2,1} W_b + k_{2,2} W_s + G^* \widetilde{W}^3 + \Psi_{2,1} W_b^* + \Psi_{2,2} W_s^* = 0 \tag{36}$$

in which $\widetilde{W} = W_b + W_s$ is such a way that W_b and W_s are maximum values of bending and shear deflections, respectively and W_b^* and W_s^* are magnitude of imperfection due to initial bending and shear deflections, respectively. Also, $k_{i,j}$ and $\Psi_{i,j}$ define linear stiffness matrix respectively for perfect and imperfect master element. Also, G^* is the nonlinear stiffness matrix of master element. Simultaneously solving the two equation for finding buckling load will give the post-buckling path of the beam. Here, calculations have been carried out according to below dimensionless factors:

$$K_L = k_L \frac{L^4}{D}, \quad K_p = k_p \frac{L^2}{D}, \quad K_{NL} = k_{NL} \frac{L^4}{A}, P = P \frac{12L^2}{E_{GOP} h^3} \tag{37}$$

Table 1 Validation of critical buckling load for a beam with epoxy matrix and GOP content

W_{GOP}		Zhang *et al*. (2020)	Present FEM solution
0.3%	L/h=10	0.0101	0.0102
	L/h=15	0.0046	0.0048
	L/h=20	0.0026	0.0028

5. Discussions and results

Based on the section, new findings have been presented for post-buckling investigation of GOP reinforced sandwich beams modeled as a refined thick structure incorporating geometric imperfectness. Before all, the critical buckling loads of GOP reinforced beams have been verified by using the data of Timoshenko beams reported by Zhang *et al*. (2020), as presented in Table 1. To do this, a S-S beam having uniform distribution of GOPs is selected. With respect to different of slenderness ratio (L/h), an excellent agreement is achieved among obtained critical buckling loads with those provided by Zhang *et al*. (2020). In the present study, the material properties of GOP reinforced beam with epoxy matrix are selected as:

- $E_{GOP} = 444.8\ GPa$, $d_{GOP} = 500\ nm$, $t_{GOP} = 0.95\ nm$, $v_{GOP} = 0.165$.
- $E_M = 3.4\ GPa$, $v_M = 0.34$.

GOP amount effects on the post-buckling characteristics of sandwich beams have been represented in Fig. 2 at imperfection amplitude of W^*/h=0.01. Uniform GOP distribution has been considered. For an ideal (perfect) GOP-reinforced beam, the starting point ($\widetilde{W}/h = 0$) highlights the critical buckling point. Moreover, for an imperfect GOP-reinforced beam ($W^*/h \neq 0$), there is not any critical buckling point, since the beam is at its primary formation. It may be understood that the nonlinear buckling load gets larger with the increasing of non-dimension deflection. This is because of the intrinsic stiffening effect. Reinforcing effect of GOPs on buckling behaviors of the beam is evidently observable from this figure. Indeed, the total stiffness of the reinforced sandwich beam may be substantially strengthened by including a slight amount of GOPs in matrix material (epoxy). Hereupon, non-linear

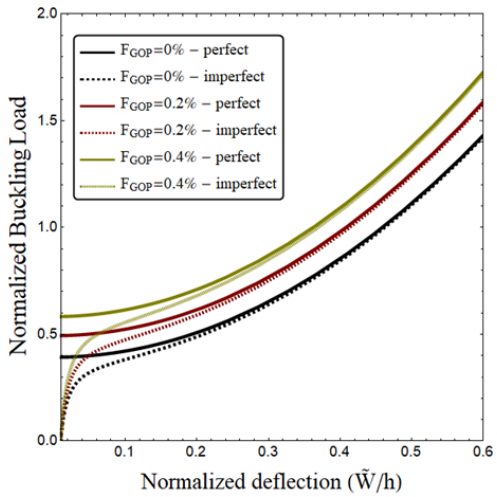

Fig. 2 Buckling load of sandwich beam against normalized deflection for different GOP weight fraction (h_f=0.2h, L/h=12, W^*/h=0.01)

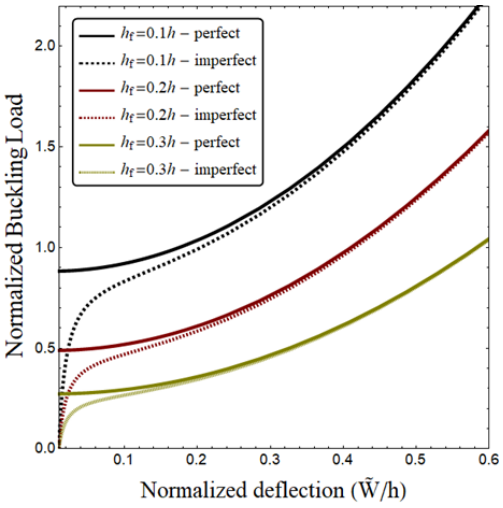

Fig. 3 Buckling load of sandwich beam against normalized deflection for different values of face sheet thickness (L/h=12, F_{GOP}=0.2%, W*/h=0.01)

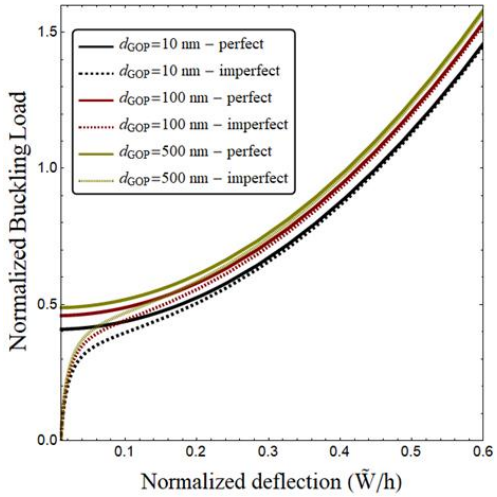

Fig. 4 Buckling load of the GOP-reinforced beam against normalized deflection for different GOP diameters (F_{GOP}=0.2%, W*/h=0.01)

stability load magnifies by the growth of GOP weight fraction (F_{GOP}).

In Fig. 3, post-buckling load-amplitude curves of a GOP-reinforced sandwich beam with and without geometric imperfections have been presented accounting for various values of face sheet thickness (h_f). It is considered that L/h=12 and W^*=0.01h. The most important point is that increasing face sheet thickness yields lower buckling loads. This is because by increasing the value of face sheet thickness, the core thickness is reduced at a fixed total thickness. It must be noted that core is made of metal (Aluminum) with higher elastic modulus compared to face sheets. Therefore, reduction in the core thickenss results in lower buckling curves.

GOP diameter (d_{GOP}) effect on post-buckling behavior of sandwich GOP-reinforced beam has been plotted in Fig. 4 via comparison of obtained results for d_{GOP}=10, 100 and 500 nm. Geometric imperfection amplitude is selected as W*/h=0.01. This figure shows that a beam with higher d_{GOP} gives higher post-buckling loads due to stiffness increment and increase of beam rigidity. It means that larger GOPs will results in higher nonlinear stability curves.

Geometric imperfectness (W^*/h) effects on post-buckling behaviors of GOP-reinforced beams are depicted in Fig. 5 selecting F_{GOP}=0.2%. An important fact is that the initial deflection of GOP-reinforced beam has huge influences on non-linear load-deflection path. According to before discussions, the critical buckling load vanishes by considering the primary geometric imperfectness. Indeed, considering perfect configurations ($W^*/h = 0$) results in critical buckling of the GOP-reinforced beam. Next, beam buckling capacity improves with the growth of non-dimension amplitudes. However, considering imperfect configurations ($W^*/h \neq 0$), results in no buckling capacity before the primary condition of the GOP-reinforced beam. An important finding is that as the magnitude of imperfection is greater, the post-buckling loads is lower.

Fig. 6 indicates the changes of non-linear buckling load of a GOP-reinforced sandwich beam against non-dimension amplitudes with respect to diverse linear (K_L), shear (K_P) and non-linear (K_{NL}) foundation factors when F_{GOP}=0.2%. An important fact is that K_P prepares a joined interplay with the GOP-reinforced beam, whereas K_L prepares a halting interplay with the beam. Augmenting foundation factors produces greater non-linear stability loads by elevating the transverse strength of the GOP-reinforced beam. A significant fact is that the impacts of non-linear foundation factor on non-linear buckling load are remarkably influenced by the geometric non-linearity or non-dimension amplitudes, whereas the impacts of K_L and K_P on buckling load are not influenced by the geometric non-linearity. Indeed, as the non-dimension amplitudes become greater, the impacts of K_{NL} on non-linear buckling load gets more announced.

Buckling curves of sandwich beam with reinforced layers against normalized deflection for diverse boundary conditions has been plotted in Fig. 7. The three boundary conditions are S-S, C-S and C-C. It can be realized from the plot that C-C boundary conditions result in a stronger support and greatest buckling curves. Accordingly, type of

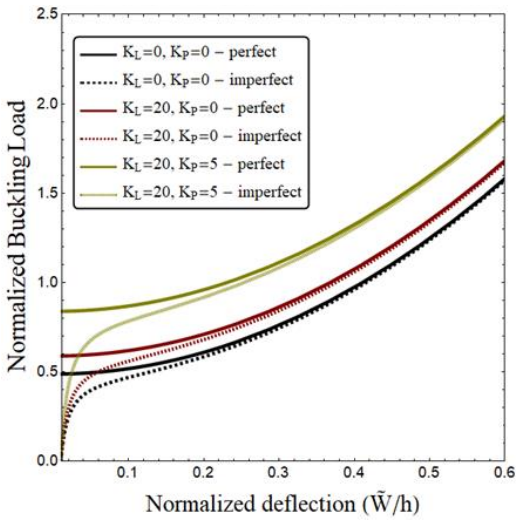

(a) Linear foundation (K_{NL}=0)

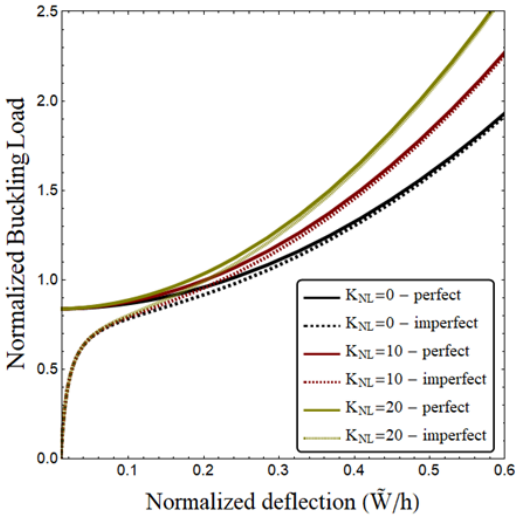

(b) Nonlinear foundation (K_L=20, K_P=5)

Fig. 6 Buckling load of the beam with uniform GOP against normalized deflection for diverse foundatio coefficients (h_f=0.2h, L/h=12, F_{GOP}=0.2 %)

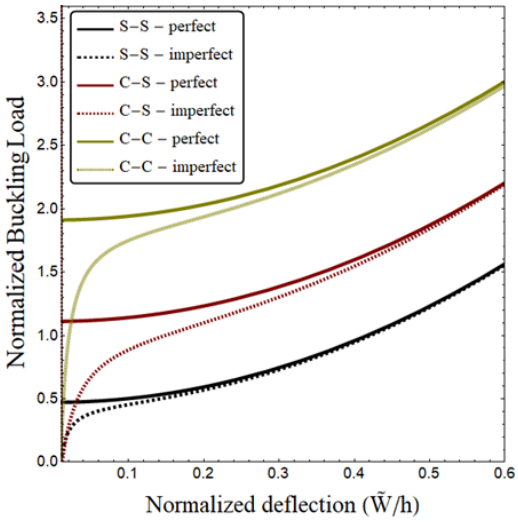

Fig. 7 Buckling load of the beam with uniform GOPs against normalized deflection for diverse boundary conditions (h_f=0.2h, L/h=12, F_{GOP}=0.2 %)

end condition has a key role on mehcanical post-buckling behavior of perfect/imperfect GOP-reinforced sandwich beams.

6. Conclusions

In the presented article, finite element (FE) simulations were developed for study on mechanical nonlinear stability of sandwich beams with GOP-reinforced skins. To this goal, a higher-order refined beam formulation was applied to model the sandwich beam with uniformly distributed GOPs. Likewise, the developed FE simulations contained refined beam elements in which shear deformations were taken into account. The most important observation was that increasing GOP weight fraction yields larger buckling loads. It means that adding the amount of GOP can increase the beam stiffness and enhance its post-buckling behavior. An important finding was that as the magnitude of imperfection is greater, the post-buckling load is lower. It was shown that a beam with higher GOP diameter gives higher post-buckling loads due to stiffness increment and increase of beam rigidity. The most important point was that increasing face sheet thickness led to lower buckling loads.

References

Abdulrazzaq, M.A., Muhammad, A.K., Kadhim, Z.D. and Faleh, N.M. (2020), "Vibration analysis of nonlocal strain gradient porous FG composite plates coupled by visco-elastic foundation based on DQM", *Couple. Syst. Mech.*, **9**(3), 201-217. https://doi.org/10.12989/csm.2020.9.3.201.

Ahankari, S.S and Kar, K.K. (2010), "Hysteresis measurements and dynamic mechanical characterization of functionally graded natural rubber–carbon black composites", *Polym. Eng. Sci.*, **50**(5), 871-877. https://doi.org/10.1002/pen.21601.

Ahmed, R.A., Fenjan, R.M., Hamad, L.B. and Faleh, N.M. (2020a), "A review of effects of partial dynamic loading on dynamic response of nonlocal functionally graded material beams", *Adv. Mater. Res.*, **9**(1), 33-48. https://doi.org/10.12989/amr.2020.9.1.033.

Ahmed, R.A., Al-Maliki, A.F. and Faleh, N.M. (2020b), "Dynamic characteristics of multi-phase crystalline porous shells with using strain gradient elasticity", *Adv. Nano Res.*, **8**(2), 157. https://doi.org/10.12989/anr.2020.8.2.157-167.

Al-Maliki, A.F., Faleh, N.M. and Alasadi, A.A. (2019), "Finite element formulation and vibration of nonlocal refined metal foam beams with symmetric and non-symmetric porosities", *Struct. Monit. Maint.*, **6**(2), 147-159. https:// doi.org/10.12989/smm.2019.6.2.147.

Barati, M.R. and Shahverdi, H. (2017), "Dynamic modeling and vibration analysis of double-layered multi-phase porous nanocrystalline silicon nanoplate systems", *Eur. J. Mech. A*, **66**, 256-268. https://doi.org/10.1016/j.euromechsol.2017.07.010.

Barati, M.R. and Shahverdi, H. (2018a), "Forced vibration of porous functionally graded nanoplates under uniform dynamic load using general nonlocal stress–strain gradient theory", *J. Vib. Control*, **24**(20), 4700-4715. https://doi.org/10.1177%2F1077546317733832.

Barati, M.R. and Shahverdi, H. (2018b), "Nonlinear thermal vibration analysis of refined shear deformable FG nanoplates: Two semi-analytical solutions", *J. Brazil. Soc. Mech. Sci. Eng.*, **40**(2), 1-15. https://doi.org/10.1007/s40430-018-0968-0.

Ebrahimi, F. and Barati, M.R. (2017a), "Dynamic modeling of

preloaded size-dependent nano-crystalline nano-structures", *Appl. Math. Mech.*, **38**(12), 1753-1772. https://doi.org/10.1007/s10483-017-2291-8.

Ebrahimi, F. and Barati, M.R. (2017b), "A third-order parabolic shear deformation beam theory for nonlocal vibration analysis of magneto-electro-elastic nanobeams embedded in two-parameter elastic foundation", *Adv. Nano Res.*, **5**(4), 313. https://doi.org/10.12989/anr.2017.5.4.313.

Ebrahimi, F. and Barati, M.R. (2017c), "A general higher-order nonlocal couple stress based beam model for vibration analysis of porous nanocrystalline nanobeams", *Superlattice Microst.*, **112**, 64-78. https://doi.org/10.1016/j.spmi.2017.09.010.

Ebrahimi, F. and Barati, M.R. (2017d), "Static stability analysis of embedded flexoelectric nanoplates considering surface effects", *Appl. Phys. A*, **123**(10), 1-15. https://doi.org/10.1007/s00339-017-1265-y.

Ebrahimi, F. and Barati, M.R. (2017e), "Electro-magnetic effects on nonlocal dynamic behavior of embedded piezoelectric nanoscale beams", *J. Intell. Mater. Syst. Struct.*, **28**(15), 2007-2022. https://doi.org/10.1177%2F1045389X16682850.

Ebrahimi, F. and Barati, M.R. (2018a), "Free vibration analysis of couple stress rotating nanobeams with surface effect under in-plane axial magnetic field", *J. Vib. Control*, **24**(21), 5097-5107. https://doi.org/10.1177%2F1077546317744719.

Ebrahimi, F. and Barati, M.R. (2018b), "Vibration analysis of nonlocal strain gradient embedded single-layer graphene sheets under nonuniform in-plane loads", *J. Vib. Control*, **24**(20), 4751-4763. https://doi.org/10.1177%2F1077546317734083.

Ebrahimi, F. and Barati, M.R. (2018c), "Hygro-thermal vibration analysis of bilayer graphene sheet system via nonlocal strain gradient plate theory", *J. Brazil. Soc. Mech. Sci. Eng.*, **40**(9), 1-15. https://doi.org/10.1007/s40430-018-1350-y.

Ebrahimi, F. and Barati, M.R. (2018d), "Static stability analysis of double-layer graphene sheet system in hygro-thermal environment", *Microsyst. Technol.*, **24**(9), 3713-3727. https://doi.org/10.1007/s00542-018-3827-0.

Ebrahimi, F. and Barati, M.R. (2018e), "Influence of neutral surface position on dynamic characteristics of in-homogeneous piezo-magnetically actuated nanoscale plates", *Proceedings of the Institution of Mechanical Engineers, Part C: Journal of Mechanical Engineering Science*, **232**(17), 3125-3143. https://doi.org/10.1177%2F0954406217728977.

Ebrahimi, F. and Barati, M.R. (2018f), "Vibration analysis of parabolic shear-deformable piezoelectrically actuated nanoscale beams incorporating thermal effects", *Mech. Adv. Mater. Struct.*, **25**(11), 917-929. https://doi.org/10.1080/15376494.2017.1323141.

Ebrahimi, F. and Barati, M.R. (2018g), "Nonlocal and surface effects on vibration behavior of axially loaded flexoelectric nanobeams subjected to in-plane magnetic field", *Arab. J. Sci. Eng.*, **43**(3), 1423-1433. https://doi.org/10.1007/s13369-017-2943-y.

Ebrahimi, F. and Barati, M.R. (2018h), "Size-dependent thermally affected wave propagation analysis in nonlocal strain gradient functionally graded nanoplates via a quasi-3D plate theory", *Proceedings of the Institution of Mechanical Engineers, Part C: Journal of Mechanical Engineering Science*, **232**(1), 162-173. https://doi.org/10.1177%2F0954406216674243.

Esawi, A.M.K., Morsi, K., Sayed, A., Taher, M and Lanka, S. (2011), "The influence of carbon nanotube (CNT) morphology and diameter on the processing and properties of CNT-reinforced aluminium composites", *Compos. Part A*, **42**(3), 234-243. https://doi.org/10.1016/j.compositesa.2010.11.008.

Fang, M., Wang, K., Lu, H., Yang, Y. and Nutt, S. (2009), "Covalent polymer functionalization of graphene nanosheets and mechanical properties of composites", *J. Mater. Chem.*, **19**(38), 7098-7105. https://doi.org/10.1039/B908220D.

Fenjan, R.M., Ahmed, R.A., Hamad, L.B. and Faleh, N.M. (2020a), "A review of numerical approach for dynamic response of strain gradient metal foam shells under constant velocity moving loads", *Adv. Comput. Des.*, **5**(4), 349-362. https://doi.org/10.12989/acd.2020.5.4.349.

Fenjan, R.M., Faleh, N.M. and Ridha, A.A. (2020b), "Strain gradient based static stability analysis of composite crystalline shell structures having porosities", *Steel Compos. Struct.*, **36**(6), 631-642. https://doi.org/10.12989/scs.2020.36.6.631.

Feng, C., Kitipornchai, S. and Yang, J. (2017), "Nonlinear free vibration of functionally graded polymer composite beams reinforced with graphene nanoplatelets (GPLs)", *Eng. Struct.*, **140**, 110-119. https://doi.org/10.1016/j.engstruct.2017.02.052.

Forsat, M., Badnava, S., Mirjavadi, S.S., Barati, M.R. and Hamouda, A.M.S. (2020), "Small scale effects on transient vibrations of porous FG cylindrical nanoshells based on nonlocal strain gradient theory", *Eur. Phys. J. Plus*, **135**(1), 1-19. https://doi.org/10.1140/epjp/s13360-019-00042-x.

Gojny, F.H., Wichmann, M.H.G., Köpke, U., Fiedler, B and Schulte, K. (2004), "Carbon nanotube-reinforced epoxy-composites: Enhanced stiffness and fracture toughness at low nanotube content", *Compos. Sci. Technol.*, **64**(15), 2363-2371. https://doi.org/10.1016/j.compscitech.2004.04.002.

Ji, X., Guo, J., Ding, D., Gao, J., Hao, L., Guo, X. and Liu, Y. (2022), "Structural characterization and antioxidant activity of a novel high-molecular-weight polysaccharide from Ziziphus Jujuba cv. Muzao", *J. Food Measurement Charact.*, **16**(3), 2191-2200. https://doi.org/10.1007/s11694-022-01288-3.

Keleshteri, M.M., Asadi, H. and Wang, Q. (2017), "Large amplitude vibration of FG-CNT reinforced composite annular plates with integrated piezoelectric layers on elastic foundation", *Thin Wall. Struct.*, **120**, 203-214. https://doi.org/10.1016/j.tws.2017.08.035.

King, J.A., Klimek, D.R., Miskioglu, I. and Odegard, G.M. (2013), "Mechanical properties of graphene nanoplatelet/epoxy composites", *J. Appl. Polym. Sci.*, **128**(6), 4217-4223. https://doi.org/10.1002/app.38645.

Kitipornchai, S., Chen, D. and Yang, J. (2017), "Free vibration and elastic buckling of functionally graded porous beams reinforced by graphene platelets", *Mater. Des.*, **116**, 656-665. https://doi.org/10.1016/j.matdes.2016.12.061.

Kunbar, L.A.H., Hamad, L.B., Ahmed, R.A. and Faleh, N.M. (2020), "Nonlinear vibration of smart nonlocal magneto-electro-elastic beams resting on nonlinear elastic substrate with geometrical imperfection and various piezoelectric effects", *Smart Struct. Syst.*, **25**(5), 619-630. https://doi.org/10.12989/sss.2020.25.5.619.

Lal, A. and Markad, K. (2018), "Deflection and stress behaviour of multi-walled carbon nanotube reinforced laminated composite beams", *Comput. Concr.*, **22**(6), 501-514. https://doi.org/10.12989/cac.2018.22.6.501.

Lin, F., Yang, C., Zeng, Q.H and Xiang, Y. (2018), "Morphological and mechanical properties of graphene-reinforced PMMA nanocomposites using a multiscale analysis", *Comput. Mater. Sci.*, **150**, 107-120. https://doi.org/10.1016/j.commatsci.2018.03.048.

Ma, X., Quan, W., Dong, Z., Dong, Y. and Si, C. (2022), "Dynamic response analysis of vehicle and asphalt pavement coupled system with the excitation of road surface unevenness", *Appl. Math. Modell.*, **104**, 421-438. https://doi.org/10.1016/j.apm.2021.12.005.

Mirjavadi, S.S., Forsat, M., Badnava, S. and Barati, M.R. (2020a), "Analyzing nonlocal nonlinear vibrations of two-phase geometrically imperfect piezo-magnetic beams considering piezoelectric reinforcement scheme", *J. Strain Anal. Eng. Des.*, **55**(7-8), 258-270. https://doi.org/10.1177%2F0309324720917285.

Mirjavadi, S.S., Forsat, M., Badnava, S., Barati, M.R. and Hamouda, A.M.S. (2020b), "Nonlinear dynamic characteristics of nonlocal multi-phase magneto-electro-elastic nano-tubes with different piezoelectric constituents", *Appl. Phys. A*, **126**(8), 1-16. https://doi.org/10.1007/s00339-020-03743-8.

Mirjavadi, S.S., Bayani, H., Khoshtinat, N., Forsat, M., Barati, M.R. and Hamouda, A.M.S. (2020c), "On nonlinear vibration behavior of piezo-magnetic doubly-curved nanoshells", *Smart Struct. Syst.*, **26**(5), 631-640. https://doi.org/10.12989/sss.2020.26.5.631.

Mirjavadi, S.S., Forsat, M., Yahya, Y. Z., Barati, M.R., Jayasimha, A.N. and Hamouda, A.M.S. (2020d), "Porosity effects on post-buckling behavior of geometrically imperfect metal foam doubly-curved shells with stiffeners", *Struct. Eng. Mech.*, **75**(6), 701-711. https://doi.org/10.12989/sem.2020.75.6.701.

Mirjavadi, S.S., Forsat, M., Mollaee, S., Barati, M.R., Afshari, B.M. and Hamouda, A.M.S. (2020e), "Post-buckling analysis of geometrically imperfect nanoparticle reinforced annular sector plates under radial compression", *Comput. Concr.*, **26**(1), 21-30. https://doi.org/10.12989/cac.2020.26.1.021.

Mirjavadi, S.S., Nikookar, M., Mollaee, S., Forsat, M., Barati, M. R. and Hamouda, A.M.S. (2020f), "Analyzing exact nonlinear forced vibrations of two-phase magneto-electro-elastic nanobeams under an elliptic-type force", *Adv. Nano Res.*, **9**(1), 47-58. https://doi.org/10.12989/anr.2020.9.1.047.

Mirjavadi, S.S., Forsat, M., Barati, M.R. and Hamouda, A.M.S. (2020g), "Investigating nonlinear forced vibration behavior of multi-phase nanocomposite annular sector plates using Jacobi elliptic functions", *Steel Compos. Struct.*, **36**(1), 87-101. https://doi.org/10.12989/scs.2020.36.1.087.

Mirjavadi, S.S., Forsat, M., Barati, M.R. and Hamouda, A.M.S. (2020h), "Post-buckling analysis of geometrically imperfect tapered curved micro-panels made of graphene oxide powder reinforced composite", *Steel Compos. Struct.*, **36**(1), 63-74. https://doi.org/10.12989/scs.2020.36.1.063.

Mirjavadi, S.S., Forsat, M., Barati, M.R. and Hamouda, A.M.S. (2020i), "Assessment of transient vibrations of graphene oxide reinforced plates under pulse loads using finite strip method", *Comput. Concr.*, **25**(6), 575-585. https://doi.org/10.12989/cac.2020.25.6.575.

Mirjavadi, S.S., Forsat, M., Barati, M.R. and Hamouda, A.M.S. (2020j), "Post-buckling of higher-order stiffened metal foam curved shells with porosity distributions and geometrical imperfection", *Steel Compos. Struct.*, **35**(4), 567-578. https://doi.org/10.12989/scs.2020.35.4.567.

Mirjavadi, S.S., Forsat, M., Yahya, Y.Z., Barati, M.R., Jayasimha, A.N. and Khan, I. (2020k), "Analysis of post-buckling of higher-order graphene oxide reinforced concrete plates with geometrical imperfection", *Adv. Concr. Constr.*, **9**(4), 397-406. https://doi.org/10.12989/acc.2020.9.4.397.

Mirjavadi, S.S., Forsat, M., Nia, A.F., Badnava, S. and Hamouda, A.M.S. (2020l), "Nonlocal strain gradient effects on forced vibrations of porous FG cylindrical nanoshells", *Adv. Nano Res.*, **8**(2), 149-156. https://doi.org/10.12989/anr.2020.8.2.149.

Mou, B. and Bai, Y. (2018), "Experimental investigation on shear behavior of steel beam-to-CFST column connections with irregular panel zone", *Eng. Struct.*, **168**, 487-504. https://doi.org/10.1016/j.engstruct.2018.04.029.

Mohammed, A., Sanjayan, J.G., Nazari, A. and Al-Saadi, N.T.K. (2017), "Effects of graphene oxide in enhancing the performance of concrete exposed to high-temperature", *Aust. J. Civil Eng.*, **15**(1), 61-71. https://doi.org/10.1080/14488353.2017.1372849.

Muhammad, A.K., Hamad, L.B., Fenjan, R.M. and Faleh, N.M. (2019), "Analyzing large-amplitude vibration of nonlocal beams made of different piezo-electric materials in thermal environment", *Adv. Mater. Res.*, **8**(3), 237-257. https://doi.org/10.12989/amr.2019.8.3.237.

Nieto, A., Bisht, A., Lahiri, D., Zhang, C and Agarwal, A. (2017), "Graphene reinforced metal and ceramic matrix composites: A review", *Int. Mater. Rev.*, **62**(5), 241-302. https://doi.org/10.1080/09506608.2016.1219481.

Rafiee, M.A., Rafiee, J., Wang, Z., Song, H., Yu, Z.Z. and Koratkar, N. (2009), "Enhanced mechanical properties of nanocomposites at low graphene content", *ACS Nano*, **3**(12), 3884-3890. https://doi.org/10.1021/nn9010472.

Rezaiee-Pajand, M., Masoodi, A. and Mokhtari, M. (2018), "Static analysis of functionally graded non-prismatic sandwich beams", *Adv. Comput. Des.*, **3**(2), 165-190. https://doi.org/10.12989/acd.2018.3.2.165.

Shariati, A., Barati, M.R., Ebrahimi, F., Singhal, A. and Toghroli, A. (2020a), "Investigating vibrational behavior of graphene sheets under linearly varying in-plane bending load based on the nonlocal strain gradient theory", *Adv. Nano Res.*, **8**(4), 265-276. https://doi.org/10.12989/anr.2020.8.4.265.

Shariati, A., Barati, M.R., Ebrahimi, F. and Toghroli, A. (2020b), "Investigation of microstructure and surface effects on vibrational characteristics of nanobeams based on nonlocal couple stress theory", *Adv. Nano Res.*, **8**(3), 191-202. https://doi.org/10.12989/anr.2020.8.3.191.

Shen, H.S., Xiang, Y., Lin, F. and Hui, D. (2017), "Buckling and postbuckling of functionally graded graphene-reinforced composite laminated plates in thermal environments", *Compos. Part B Eng.*, **119**, 67-78. https://doi.org/10.1016/j.compositesb.2017.03.020.

Song, M., Kitipornchai, S. and Yang, J. (2017), "Free and forced vibrations of functionally graded polymer composite plates reinforced with graphene nanoplatelets", *Compos. Struct.*, **159**, 579-588. https://doi.org/10.1016/j.compstruct.2016.09.070.

Xiao, G., Chen, B., Li, S. and Zhuo, X. (2022), "Fatigue life analysis of aero-engine blades for abrasive belt grinding considering residual stress", *Eng. Fail. Anal.*, **131**, 105846. https://doi.org/10.1016/j.engfailanal.2021.105846.

Xiong, Q.M., Chen, Z., Huang, J.T., Zhang, M., Song, H., Hou, X. F. and Feng, Z.J. (2020), "Preparation, structure and mechanical properties of Sialon ceramics by transition metal-catalyzed nitriding reaction", *Rare Metals*, **39**(5), 589-596. https://doi.org/10.1007/s12598-020-01385-6.

Yan, Y., Feng, L., Shi, M., Cui, C. and Liu, Y. (2020), "Effect of plasma-activated water on the structure and in vitro digestibility of waxy and normal maize starches during heat-moisture treatment", *Food Chem.*, **306**, 125589. https://doi.org/10.1016/j.foodchem.2019.125589.

Yang, B., Yang, J. and Kitipornchai, S. (2017), "Thermoelastic analysis of functionally graded graphene reinforced rectangular plates based on 3D elasticity", *Meccanica*, **52**(10), 2275-2292. https://doi.org/10.1007/s11012-016-0579-8.

Zhang, Z., Li, Y., Wu, H., Zhang, H., Wu, H., Jiang, S. and Chai, G. (2020), "Mechanical analysis of functionally graded graphene oxide-reinforced composite beams based on the first-order shear deformation theory", *Mech. Adv. Mater. Struct.*, **27**, 3-11. https://doi.org/10.1080/15376494.2018.1444216.

CC